Structure and transport properties of the quasi-one-dimensional telluride $Ta_{1.2}Os_{0.8}Te_4$

Wen-He Jiao,[1,*] Shaozhu Xiao,[2] Shi-Ju Zhang,[2] Wu-Zhang Yang,[3,4] Xiao-Meng Xie,[5] Yi Liu,[1] Ji-Yong Liu,[6] Shi-Jie Song,[7] Wei Liu,[2] Zhi Ren,[3,4] Guang-Han Cao,[7] Xiaofeng Xu,[1,†] and Shaolong He[2,8,‡]

[1]*Key Laboratory of Quantum Precision Measurement of Zhejiang Province, Department of Applied Physics, Zhejiang University of Technology, Hangzhou 310023, China*

[2]*Ningbo Institute of Materials Technology and Engineering, Chinese Academy of Sciences, Ningbo 315201, China*

[3]*Key Laboratory for Quantum Materials of Zhejiang Province, School of Science, Westlake University, Hangzhou 310024, China*

[4]*Institute of Natural Sciences, Westlake Institute for Advanced Study, Hangzhou 310024, China*

[5]*Department of Applied Physics, Zhejiang University of Science and Technology, Hangzhou 310023, China*

[6]*Department of Chemistry, Zhejiang University, Hangzhou 310027, China*

[7]*Department of Physics, Zhejiang Province Key Laboratory of Quantum Technology and Devices, Interdisciplinary Center for Quantum Information, and State Key Lab of Silicon Materials, Zhejiang University, Hangzhou 310027, China*

[8]*Center of Materials Science and Optoelectronics Engineering, University of Chinese Academy of Sciences, Beijing 100049, China*

(Received 30 August 2021; revised 20 November 2021; accepted 25 January 2022; published 2 February 2022)

We report the crystal growth, structural characterization, and physical properties of an off-stoichiometric van der Waals telluride $Ta_{1.2}Os_{0.8}Te_4$, which is isostructural with the noncentrosymmetric WTe_2, a prototypical type-II Weyl semimetal. Transport measurements have been carried out in magnetic fields up to 9 T. A low-temperature resistivity upturn is observed along all three crystallographic directions at zero field. The along-chain ρ_a and interchain ρ_b are found to increase logarithmically at low temperatures, while in the low-T metallic regime, both longitudinal and transverse transports support a three-dimensional Fermi liquid ground state. As temperature is further increased, successive crossovers to electronic states of reduced dimensionality can be seen in both interchain resistivities. The transverse magnetoresistance is weak but anisotropic, the analysis of which indicates the Kohler's rule is severely violated over a large temperature range. The positive linear field dependence of Hall resistivity at selected temperatures indicates the dominance of single-band hole-type charge carriers, consistent with the results of the angle-resolved photoemission spectroscopy. Our results not only establish this transition-metal telluride family as a good system for studying various dimensional crossover phenomena, but also offer the potential for exploring topologically nontrivial phases with reduced dimensionality, given its structural similarity to WTe_2.

DOI: 10.1103/PhysRevB.105.064201

I. INTRODUCTION

A vast class of two-dimensional (2D) van der Waals (vdW) layered materials has been found and extensively studied in past decades [1], because such materials not only exhibit a wealth of fascinating physics, such as superconductivity [2,3], robust ferroelectricity [4], and novel topological states [5], but also have widespread applications in fields ranging from electronics/optoelectronics, quantum mechanical devices to electrochemical catalysis [6,7]. Low-dimensional structure as a common feature of vdW layered materials is a key ingredient in realizing potential applications and may also play a significant role in exotic quantum physics therein. If the dimensionality of materials is further reduced, low-dimensional interacting electron systems may lead to more exotic physical phenomena, including charge/spin density waves (CDW/SDW), Wigner electronic crystals, diverse forms of charge order, or even unconventional superconductivity, etc. [8]. Strikingly, Fermi liquid (FL) theory, which is applicable in most three-dimensional (3D) systems, breaks down when electrons are spatially confined into one-dimensional (1D) limit, leading to the spin-charge separation no matter how weak the electron-electron interactions are [9,10], a hallmark of the Tomonaga-Luttinger (TL) liquid. In real electronic systems, however, purely 1D conduction is not strict but coupling has to exist between chains, leading to the so-called quasi-1D conductors. Provided that the two orthogonal interchain hopping energies $2t_\perp$ are small enough with respect to the external perturbations, dimensional crossover phenomena could be observed as a function of both temperature and magnetic field [8], as reported in quasi-1D cuprates [11,12] and Bechgaard salt $(TMTSF)_2PF_6$ [13,14]. It was claimed that any finite $2t_\perp$ would stabilize the metallic state [15], and according to the renormalization group theory, the metallic state also forms a 3D FL ground state [16]. However, Prigodin and Firsov (PF) argued that quasi-1D conductors would become effectively 1D in the case of intrachain impurity scattering rates satisfying $\hbar/\tau_0 > 2t_\perp$ and,

*whjiao@zjut.edu.cn
†xuxiaofeng@zjut.edu.cn
‡shaolonghe@nimte.ac.cn

therefore, susceptible to electron localization at low temperatures [17].

The layered transition-metal tellurides (TMTs) represent one class of vdW layered materials, the atomic layers of which are composed of multiple kinds of alternating quasi-1D chains [18]. Recently, distinctive physical properties have been reported among ternary TMTs, such as superconductivity in $Ta_4Pd_3Te_{16}$ and $Ta_3Pd_3Te_{14}$ [19,20]; topological Dirac state in $TaPdTe_5$, $TaPtTe_5$, $TaNiTe_5$, and $TaNi_2Te_3$ [21–24]; and the type-II Weyl state in noncentrosymmetric (Ta, Nb)$IrTe_4$ [25–27]. More intriguingly, unconventional surface superconductivity with onset T_c up to 1.54 K, which also exhibits quasi-1D and topologically nontrivial characteristics, was claimed in $TaIrTe_4$, demonstrating that $TaIrTe_4$ may be a unique candidate of topological superconductors [28]. Remarkably, the ferroelectriclike polarizations, possibly originating from a noncentrosymmetric reconstruction of the surface atoms, together with Dirac-like surface state were recently observed in $TaNiTe_5$ [29]. These observations further motivate us to synthesize new compounds and explore their novel physical properties among TMTs.

In this work, we report the crystal growth, structural characterization, and physical properties of an off-stoichometric vdW telluride $Ta_{1.2}Os_{0.8}Te_4$. The 2D atomic layer comprises alternating arrays of $TaTe_2$ and $OsTe_2$ chains, isostructural to the type-II Weyl semimetal WTe_2 [30,31], but with 20% extra Ta atoms occupying the Os sites, resulting in a molar ratio Ta : Os : Te = 1.2 : 0.8 : 4. The two interchain resistivities ρ_b and ρ_c show a metal-insulator transition at different temperatures, indicating successive crossovers from 3D to 1D with increasing temperature. The low-T upturn of the resistivities is observed along all three crystallographic directions, the possible origins of which are thoroughly discussed. Collectively, our results suggest that the coupling between chains in $Ta_{1.2}Os_{0.8}Te_4$ leads to a 3D FL ground state, in favor of the renormalization group theory, and electrons become localized at low temperatures, which is responsible for the resistivity upturn seen in this material.

II. EXPERIMENTAL METHODS

A. Sample synthesis

Single crystals of $Ta_{1.2}Os_{0.8}Te_4$ were grown via a self-flux method, similar to that in growing $TaPdTe_5$ and $TaPtTe_5$ single crystals [21,22]. Powders of the elements Ta (99.97%), Os (99.95%), and Te (99.99%), in an atomic ratio of Ta : Os : Te = 1 : 1 : 10, were thoroughly ground by hand in agate mortar. Then, the mixture was loaded, and sealed into an evacuated quartz ampule. All the procedures handling the reagents were done in a glovebox filled with pure argon gas (O_2 and H_2O < 0.1 ppm). The ampoule was slowly heated up to 1273 K and held for 48 h. After that, it was cooled to 773 K at a rate of 6 K/h, then followed by furnace-cooling down to room temperature. Small shiny gray-black flattened needlelike crystals with a typical size of $1.5 \times 0.3 \times 0.1$ mm^3 were harvested [see the left inset of Fig. 1(a)]. The air-stable crystals are malleable, and can be easily exfoliated to a thin layer by a razor blade.

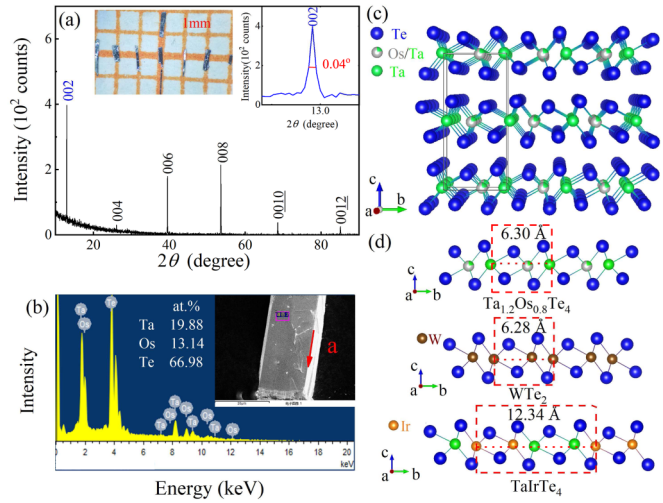

FIG. 1. Sample characterizations and crystallographic structure of $Ta_{1.2}Os_{0.8}Te_4$. (a) Single-crystal x-ray diffraction pattern. The left inset is a photograph of the $Ta_{1.2}Os_{0.8}Te_4$ crystals on a millimeter-grid paper. The right inset shows the first reflection in x-ray diffraction pattern. (b) A typical energy-dispersive x-ray spectrum with electron beams focused on the selected area (marked in the inset) of the crystals. (c) Crystal structure of $Ta_{1.2}Os_{0.8}Te_4$ viewed perspectively along the a axis. (d) Projection view of one atomic layer of $Ta_{1.2}Os_{0.8}Te_4$ (upper), WTe_2 (middle), and $TaIrTe_4$ (bottom) along the chain direction.

B. Structure and composition determination

The actual chemical composition of the as-grown crystals was determined by energy-dispersive x-ray spectroscopy (EDS) with an AMETEK©EDAX (Model Octane Plus) spectrometer, equipped in a field-emission scanning electron microscope (Hitachi S-4800). We arbitrarily selected four pieces of crystals from the same batch for the EDS measurement to obtain the average stoichiometry. Figure 1(b) shows the typical EDS spectrum for a piece of crystal. The average chemical composition of the as-grown crystals is determined to be $Ta_{1.20}Os_{0.79}Te_{4.04}$ by fixing the Ta content to be 1.20. The detailed results are tabulated in Table S1 of the Supplemental Material (SM) [32].

X-ray diffraction (XRD) data collection from this single crystal was performed on an Xcalibur, Atlas, Gemini ultra diffractometer. The crystal was mounted on the CCD goniometer head, followed by diffraction data collections at 170.15 K. Data collection, integration, and absorption correction were done in the X-AREA software package. The structure was solved by a direct method and refined by full-matrix least squares based on F^2 using a SHELXTL program package [33]. The result indicates our crystals adopt a noncentrosymmetric orthorhombic structure with the space group $Pmn2_1$ (No. 31). Its atomic coordinates and thermal displacement parameters (U_{eq}) are given in Tables S2 and S3 of the SM. The related bond lengths and bond angles are given in Tables S4 and S5 of the SM. Single-crystal XRD data collection was also performed at room temperature with a monochromatic Cu $K\alpha 1$ radiation using a PANalytical x-ray diffractometer (model EMPYREAN) radiation by a conventional θ-2θ scan for a crystal mounted on a sample holder. As shown in Fig. 1(a),

TABLE I. Crystallographic data and experiment details for $Ta_{1.2}Os_{0.8}Te_4$

Compound	$Ta_{1.2}Os_{0.8}Te_4$
T of data collection (K)	170.15
Wavelength (Å)	0.71073
Formula weight (g mol^{-1})	879.70
Crystal system	Orthorhombic
Space group	$Pmn2_1$
a (Å)	3.6034(7)
b (Å)	6.3042(12)
c (Å)	13.674(2)
Volume (Å^3)	310.63(10)
Z	1
Density (calculated) (g cm^{-3})	9.405
μ (mm^{-1})	55.733
$F(000)$	731.0
Crystal size (mm^3)	0.1 × 0.1 × 0.088
2θ range for data collection (deg)	5.958 to 55.978
Index ranges	$-4 \leqslant h \leqslant 4$
	$-8 \leqslant k \leqslant 8$
	$-18 \leqslant l \leqslant 18$
Reflection collected	852
Independent reflections	852 [$R_{\rm int} = 0.0636$]
Data/restraints/parameters	852/1/38
Goodness of fit	1.084
Final R[a] indices [$>2\sigma(I)$]	$R_{\rm obs} = 0.0520$
	$\omega R_{\rm obs} = 0.1457$
R indices (all data)	$R_{\rm all} = 0.0527$
	$\omega R_{\rm all} = 0.1469$

[a]$R = \Sigma||F_o|-|F_c||/\Sigma|F_o|$, $\omega R = \{\Sigma[\omega(|F_o|^2-|F_c|^2)^2]/\Sigma[\omega(|F_o|^4)]\}^{1/2}$, and $\omega = 1/[\sigma^2(F_o^2) + (0.0894P)^2 + (22.44P)]$, where $P = (F_o^2 + 2F_c^2)/3$.

only multiple peaks arising from the diffraction from (0 0 l) planes can be observed, consistent with the layered crystal structure. The left inset of Fig. 1(a) shows the first reflection (the maximum peak), full width at half-maximum of which is only 0.04°, indicating the high quality of the crystals. The interplane spacing at room temperature is determined to be 6.836 Å, and this value is very close to half of the lattice parameter c ($c/2 = 6.837$ Å) tabulated in Table I.

C. Physical property measurements

Magnetic susceptibility measurements were performed on a commercial Quantum Design magnetic property measurement system (MPMS-7). The electrical resistivity and magnetoresistivity measurements were carried out in a physical property measurement system (PPMS-9; Quantum Design) with ac transport option (typical excitation current 1 mA). Gold wires were attached to the crystals by silver paste with a standard four-probe method. The electrode configurations for measuring the resistance along all three directions are illustrated in the insets of Figs. 2(a), 2(b) and 2(c), respectively. The Hall-effect measurement was performed by reversing the field direction and antisymmetrizing the data. A traditional angle-resolved photoemission spectroscope (ARPES) with a helium lamp (photon energy $h\nu = 21.2$ eV) and a base pressure better than 5×10^{-11} mbar was utilized to measure the band structure of the samples, and measurements were performed on a fresh (001) surface of a separate crystal from the same batch, which was obtained by cleaving *in situ* at ∼7 K. During ARPES measurements, the sample temperature was kept at ∼7 K.

III. RESULTS

The crystal structure of $Ta_{1.2}Os_{0.8}Te_4$ is displayed in Fig. 1(c), which clearly shows the vdW stacking of the 2D layers along the c axis. The layered slab, as shown in the upper panel of Fig. 1(d), comprises two alternating 1D chains (Ta octahedra and adjacent edge-sharing Os octahedra) that run parallel to the a axis. This type of coordination is quite common among the tellurides, but the special point here is the partial occupation at the atomic site of Os by Ta, making the title compound off-stoichiometric. If replacing both Ta and Os with W, the WTe_2 phase would be derived [middle panel of Fig. 1(d)]. $Ta_{1.2}Os_{0.8}Te_4$ and WTe_2 have similar lattice parameters. Actually, $Ta_{1.2}Os_{0.8}Te_4$ is also isostructural with type-II Weyl semimetals (Ta, Nb)$IrTe_4$ [25–27,34] [bottom panel of Fig. 1(d)]. The major difference in terms of the crystal structure between $Ta_{1.2}Os_{0.8}Te_4$ and (Ta, Nb)$IrTe_4$ is that for the latter, it is two kinds of double octahedral chains alternating along the b axis that constitute the layered slab. Therefore, the lattice parameter b of the latter is almost twice that of the former. The distinct atomic layers of $Ta_{1.2}Os_{0.8}Te_4$, WTe_2, and $TaIrTe_4$ are plotted together in Fig. 1(d) for comparison. In the literature, the hints of this new structure among ternary TMTs can be found. A recent report on the successful growth of $Ta_{1.26}Ru_{0.75}Te_4$ single crystal, which is also an off-stoichiometric telluride [35], shows that the unit cell of $Ta_{1.26}Ru_{0.75}Te_4$ is halved along b compared to $TaIrTe_4$, found by a selected area electron diffraction (SAED) pattern. They obtained a better fit with the SAED pattern by using the proposed structure [35], the same as that of $Ta_{1.2}Os_{0.8}Te_4$ here. A much earlier work on the synthesis of $TaRuTe_4$ also reported the anomaly related to the absence of the weak $k = 2n + 1$ reflections in a long-exposure Weissenberg photograph that are expected from the structure of $TaIrTe_4$ [34]. Since the Os sites are partially occupied by Ta in our samples, one may expect the different chemical composition of $Ta_{1+x}Os_{1-x}Te_4$ other than $x = 0.2$; however, our preliminary attempts by varying Ta : Os nominal ratio to harvest $Ta_{1+x}Os_{1-x}Te_4$ crystals with the same structure of $Ta_{1.2}Os_{0.8}Te_4$, were unsuccessful.

The partial occupation in $Ta_{1.2}Os_{0.8}Te_4$ can bring about a profound impact to its macroscopic properties, as the extra Ta at the Os site behaves as disorder. The electrical resistivity, measured with the current applied along three crystallographic directions is demonstrated in Figs. 2(a)–2(c). As seen, the along-chain resistivity $\rho_a(T)$ shows metallic behavior from room temperature down to $T^a_{\rm min} = 8.4$ K, below which a low-T upturn appears. The metallic data between 45 K and $T^a_{\rm min}$ can be well fitted by $\rho_{FL} = \rho_0 + AT^2$. The residual resistivity ρ_0, obtained from the extrapolation to 0 K, is 0.27 mΩ cm. The intrachain mean-free path l_0 can be estimated to be 20.63 Å from ρ_0 using the Drude formula for a 1D metal $l_0 = \pi\hbar bc/2e^2\rho_0$, where $b = 6.30$ Å and $c = 13.67$ Å are lattice constants. Since the a-axis lattice

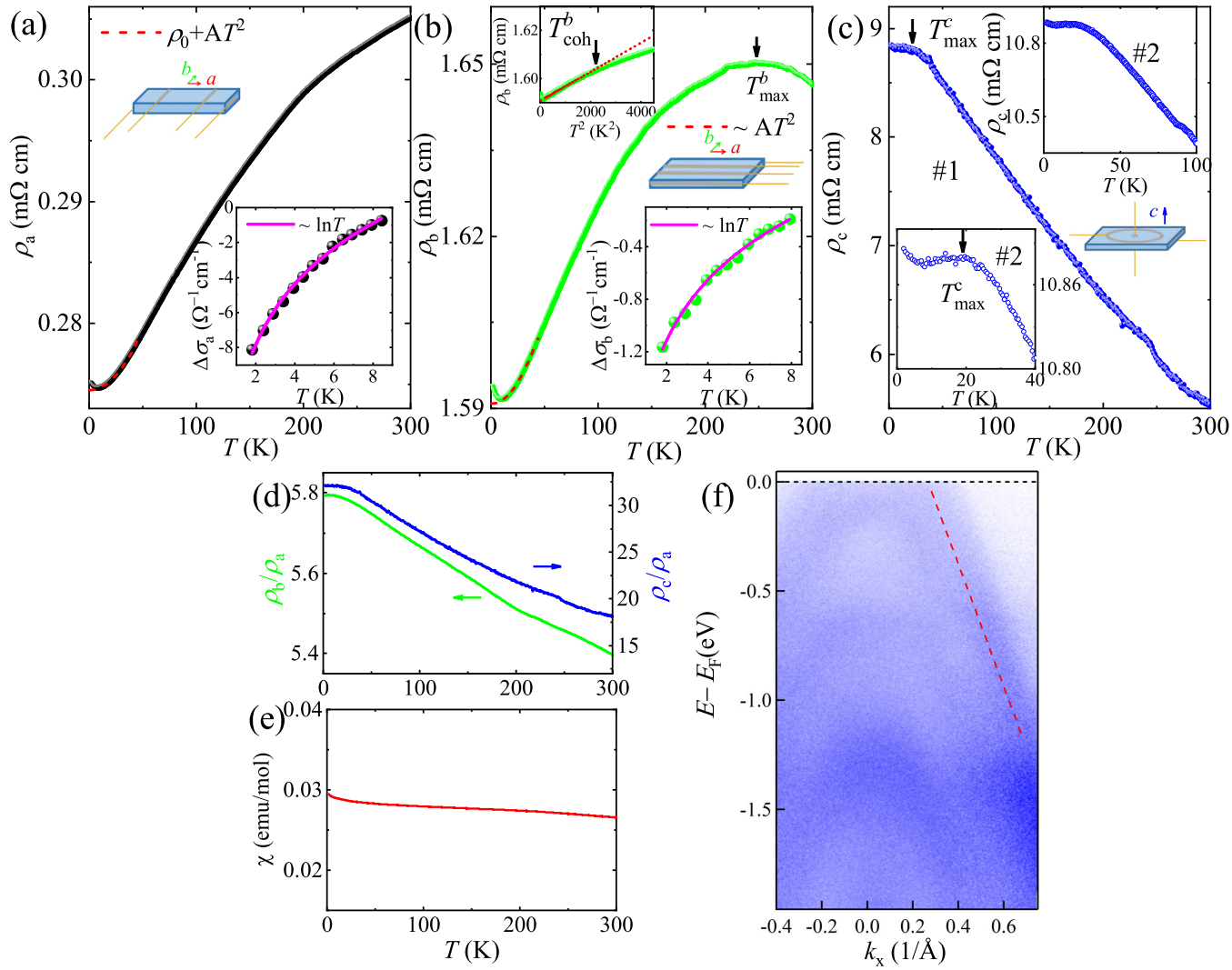

FIG. 2. Physical properties of $Ta_{1.2}Os_{0.8}Te_4$. (a)–(c) Temperature dependence of the electronic resistivity ρ_a, ρ_b, and ρ_c (crystal #1) with the current applied along the a axis (a), b axis (b), and c axis (c), respectively. The bottom inset of (a) and (b) is $\Delta\sigma$ vs T. The upper inset of (b) shows low-T data plotted against T^2, and the arrow indicates the onset of deviation from T^2 resistivity. The upper inset of (c) shows $\rho_c(T)$ measured with the other crystal #2, and the bottom inset is an enlarged view of the low-T regime. (d) Temperature dependence of the resistivity anisotropy for ρ_b/ρ_a (left axis) and ρ_c/ρ_a (right axis). (e) Temperature dependence of the magnetic susceptibility $\chi(T)$, measured at 0.5 T with field parallel to the c axis. (f) ARPES band structure at 7 K along Γ-X high symmetry direction corresponding to the intrachain direction in real space. The red dashed line indicates the band that crosses the Fermi level.

constant is 3.60 Å, l_0 is equivalent to only six unit cells. The small residual resistivity ratio RRR $= \rho_a(300\ \mathrm{K})/\rho_0 =$ 1.1 further demonstrates $Ta_{1.2}Os_{0.8}Te_4$ being a bad metal, possibly induced by intrinsic disorder. When the current is passing perpendicular to the chain direction, the resistivities ρ_b and ρ_c monotonically increase with lowering temperature, indicating a semiconducting regime before peaking at $T^b_{\mathrm{max}} =$ 248.0 K (ρ_b) and $T^c_{\mathrm{max}} = 19.0$ K (ρ_c). As shown in Fig. 2(c), $\rho_c(T)$ measured on one crystal #1 is too noisy to identify the detailed behaviors, especially at low temperatures. We therefore used a second crystal #2 to measure $\rho_c(T)$ below 100 K, shown in the upper inset of Fig. 2(c). #1 and #2 have comparable values and similar $\rho_c(T)$ profiles, indicating the reliability of our measurements. From the enlarged view in the low-T range of $\rho_c(T)$ shown in the bottom inset, we can easily identify the crossover from high-T semiconducting behavior to low-T metallic behavior, although the metallic temperature range is quite narrow. Similar behaviors have also been observed in quasi-1D cuprate $PrBa_2Cu_4O_8$ [11,36] and $(TMTSF)_2PF_6$ [13] and were attributed to a dimensional crossover with increasing temperature from 3D to 1D due to coherent to incoherent inte-chain hopping, although the dimensional crossover is usually understood as the interplay between a characteristic length of the measurements and the sample's physical dimensions [37]. Similar to a FL behavior of $\rho_a(T)$ in the metallic regime at low temperatures, both $\rho_b(T)$ and $\rho_c(T)$ in this regime also follow a quadratic temperature dependence, i.e., between 45 K and T^b_{min} for ρ_b and between 19 K and T^c_{min} for ρ_c (fit not shown here), although the metallic temperature range of ρ_c is too limited to make a solid claim. Typically, there are two energy scales that are used as a measure of $2t_\perp$ in the interchain resistivities of low-

dimensional metals, which have been experimentally verified to be feasible [12,36]. The peak in $\rho_\perp(T)$ at $T^{b,c}_{\max}$ is generally regarded as an upper bound for $2t_\perp$, while the deviation from the low-T quadratic resistivity gives a lower bound. The arrow in the upper inset of Fig. 2(b) indicates the temperature $T^b_{\rm coh}$, at which $\rho_b(T)$ first deviates from a T^2 behavior. The metallic regime below $T^c_{\max}$ is so limited that we can neglect the small difference between $T^c_{\max}$ and $T^c_{\rm coh}$ and regard them as the same. $T^{b,c}_{\rm coh}$ defines the temperature at which b- and c-axis hopping first begins to lose coherence. $T^{b,c}_{\max}$, in contrast, represent the temperature at which all interchain coherence gets lost. In the intermediate regime $T^{b,c}_{\rm coh} \leqslant T \leqslant T^{b,c}_{\max}$, the chains are weakly coupled and the metallicity disappears gradually with increasing temperature. By assuming $k_B T_{\rm coh} \approx 2t_\perp$, we obtain estimates for the warping parameters of the quasi-1D Fermi sheets: $2t^b_\perp \approx 3.88$ meV and $2t^c_\perp = 1.64$ meV.

The low-T upturn is also observed in $\rho_b(T)$ below $T^b_{\min} = 8.9$ K and $\rho_c(T)$ below $T^c_{\min} = 7.9$ K. The similar upturns have also been reported in some other compounds. For example, in purple bronze $Li_{0.9}Mo_6O_{17}$, a resistivity upturn prior to the superconducting transition was observed, the origin of which remains as yet elusive [38], with CDW/SDW, strong localization, and excitonic insulator all put forward as the possible mechanisms for this metal-insulator crossover [39]. Rather, in the highly one-dimensional cluster chain compound $Na_{2-x}Mo_6Se_6$, its resistivity upturn follows the variable range hopping law [40]. In order to gain further understanding of the nature of the upturns observed here, we now turn to a quantitative analysis by examining the correction term $\Delta\sigma_{a,b} = 1/\sigma_{a,b} - 1/\rho_{FL}$, where $\rho_{FL} = \rho_0 + AT^2$ is the red dashed line shown in panels (a) and (b) of Fig. 2. The data appear not to follow the temperature dependence expected for several mechanisms, including various types of variable range hopping conduction [$\propto \exp(-T_0/T)^\alpha$ with $\alpha = 1/2, 1/3, 1/4$] [41], thermal activation [$\propto \exp(-E_a/k_BT)$], 1D weak localization (WL) corrections ($\propto T^{-\beta/2}$, where $\beta = 2$ is the exponent in the temperature variation of the inelastic scattering time) [42], and WL correction for a TL liquid ($\propto T \ln T$) [43]. Instead, the data exhibit a $\ln T$ divergence [$\Delta\sigma_{a,b} \propto \ln T$], as shown in the bottom insets of panels (a) and (b) of Fig. 2, expected for Kondo scattering [44]. However, it is necessary to have enough magnetic impurities to induce a Kondo effect. The nearly T-independent magnetic susceptibility, plotted in Fig. 2(e), obviously argues against this Kondo mechanism but rather suggests a different origin. We shall return to this issue later.

The temperature dependence of resistivity anisotropy ρ_b/ρ_a (left axis) and ρ_c/ρ_a (right axis) is plotted in Fig. 2(d). Both ρ_b/ρ_a and ρ_c/ρ_a increase almost linearly with decreasing temperature, and flatten out at low temperatures, especially below $T^{a,b,c}_{\min}$, reflecting the same logarithmical dependence. The quasi-1D transport behaviors are exhibited with $\rho_a : \rho_b : \rho_c = 1 : 5.4 : 18.1$ at 300 K, and $1 : 5.8 : 32.1$ at 1.8 K, although the in-plane anisotropy is small compared with other quasi-1D conductors. The band structure of $Ta_{1.2}Os_{0.8}Te_4$ at ~7 K along Γ-X high symmetry direction is shown in Fig. 2(f), from which four bands are clearly resolved. Three of them exhibit holelike parabolic shape and do not cross the Fermi level. The only one that crosses the Fermi level has a nearly linear dispersion, as indicated by a red dashed line in Fig. 2(f). The slope of the linear dispersion is ~2.9 eV Å, corresponding to a very high Fermi velocity v_F of $\sim 4.4 \times 10^5$ ms^{-1} (about half of that in graphene). The linear dispersive band crosses the Fermi level at 0.34 Å^{-1}. If the Fermi pocket is assumed to be spheroidal, the 3D carrier density can be deduced from the volume of the Fermi pocket to be $\sim 1.3 \times 10^{21}$ cm^{-3}. The metallic parameter $k_F l_0$ is then estimated to be 7.8 at ~7 K, in which the Fermi wave vector k_F is 0.38 Å^{-1}, calculated from the relation $k_F = m_e v_F/\hbar$. In quasi-1D cuprate $PrBa_2Cu_4O_8$ [42], a crossover from a FL behavior to low-T localization with the current along all three crystallographic axes is also observed. By introducing intrinsic disorder through irradiation in $PrBa_2Cu_4O_8$, a localization threshold, consistent with theoretical predictions for a disorder-induced 3D-1D transition, was found to occur simultaneously along all three axes once $l_0 < 300$ Å or $k_F l_0 < 60$. Indeed, in $Ta_{1.2}Os_{0.8}Te_4$, both l_0 (20.63 Å) and $k_F l_0$ (7.8) are small enough to account for the low-T localized state. In addition, according to PF's scenario, localization in quasi-1D conductors should occur once $\hbar/\tau_0 > 2t_\perp$ [17]. For $Ta_{1.2}Os_{0.8}Te_4$, $\hbar/\tau_0 = \hbar v_F/l_0 \sim 140$ meV is far more than $2t^{b,c}_\perp$. Therefore, the low-T resistivity upturn in $Ta_{1.2}Os_{0.8}Te_4$ is overall consistent with the PF's scenario.

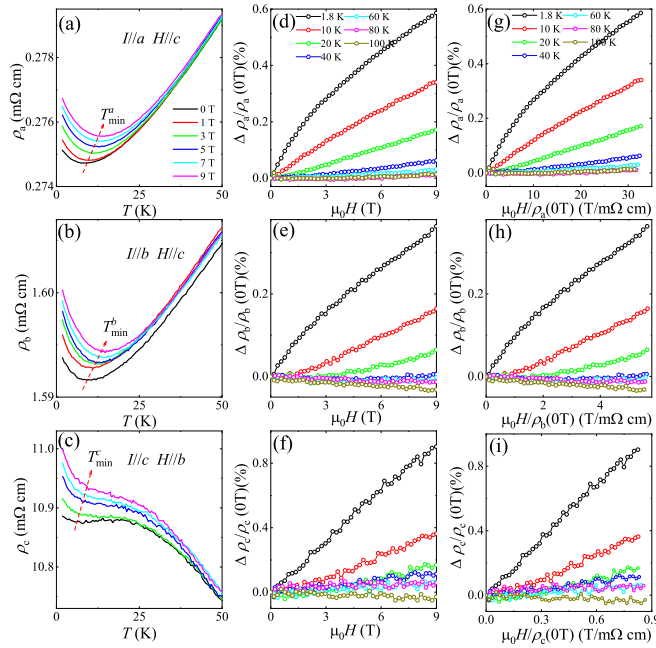

FIG. 3. Temperature dependence of ρ_a (a), ρ_b (b), and ρ_c (c) with the magnetic fields parallel to the c axis, c axis, and b axis, respectively, up to 9 T below 50 K. The transverse magnetoresistance for ρ_a (d), ρ_b (e), and ρ_c (f) at selected temperatures. Kohler's scaling for ρ_a (g), ρ_b (h), and ρ_c (i).

Figure 3 shows the transverse magnetoresistance (TMR) under different current and magnetic field configurations. The low-T upturn of ρ_a, ρ_b, and ρ_c is enhanced and $T^{a,b,c}_{\min}$ shifts towards higher temperatures with increasing field [see panels (a)–(c)]. In panels (d)–(f), we plot the TMR curves measured at fixed temperatures. In the metallic temperature range, all TMR are quite small and vary quadratically with field, as in a

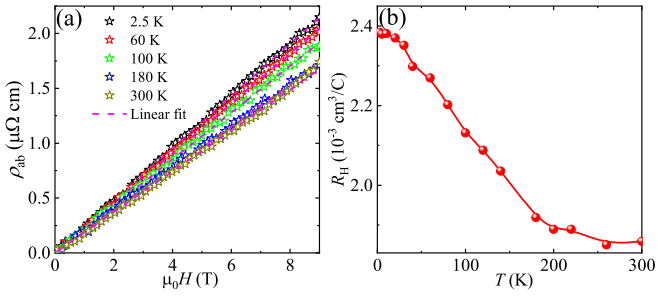

FIG. 4. (a) The Hall resistivity of $Ta_{1.2}Os_{0.8}Te_4$ at selected temperatures below 300 K. The magenta dashed lines are linear fits. (b) The temperature dependence of Hall coefficients extracted by the linear fitting.

standard metal. At temperatures below $T_{\min}^{a,b,c}$, however, TMR shows anomalous field dependence. For the current parallel to the c axis and magnetic field parallel to the b axis, the Boltzmann transport theory for a quasi-1D metal gives $\Delta\rho_c/\rho_c = (e\mu_0 Hc/\hbar)^2 l_0^2$, where c is the lattice constant [42]. At 9 T and 1.8 K, $\Delta\rho_c/\rho_c = 0.009$, giving $l_0 = 50.6$ Å, slightly larger than that estimated from the zero field ρ_0. Panels (g)–(i) of Fig. 3 show Kohler's plots for all three configurations, from which we can clearly observe that Kohler's rule is severely violated at all temperatures. Such violation of Kohler's rule is reminiscent of that observed in disordered $PrBa_2Cu_4O_8$ when $\hbar/\tau_0 > 2t_\perp$ [45], and also similar to the high-T_c cuprates $YBa_2Cu_3O_{7-\delta}$ and $La_2Sr_xCuO_4$ [46]. In these cases, such violation was attributed to the anomalous scattering time, possibly related to spin-charge separation, a hallmark of the TL state.

The Hall resistivity ρ_{ab} up to 9 T at selected temperatures below 300 K is shown in Fig. 4(a). The positive ρ_{ab} increasing almost linearly with field, suggests the dominance of single-band hole-type charge carriers, consistent with the ARPES results shown in Fig. 2(f). By linearly fitting the data, we get the T-dependent Hall coefficient R_H, as summarized in Fig. 4(b). The value $R_H = 2.4 \times 10^{-3}$ cm^3 C^{-1} at 2.5 K corresponds to a carrier concentration $n = 2.6 \times 10^{21}$ cm^{-3} by the relation $R_H = 1/ne$. Then, k_F is calculated to be 0.43 Å^{-1}, very close to the APRES results. In a purely 1D metal, no Hall voltage is expected as the Lorentz force cannot bend a trajectory of a charge carrier across the conducting chains. The Hall conductivity should remain quite small for an open Fermi surface, even if a finite $2t_\perp$ exists [47]. At low temperatures where $2t_\perp$ is much larger than k_BT, the system begins to show a quasi-2D nature, and consequently the Lorentz force becomes effective to increase R_H. Indeed, R_H of $Ta_{1.2}Os_{0.8}Te_4$ rapidly increases below $T_{\max}^b$ and eventually saturates below 30 K. A similar T-dependent R_H was also observed in quasi-1D cuprates $PrBa_2Cu_3O_7$ [48] and $PrBa_2Cu_4O_8$ [49]. Thus, T-dependent R_H can be well understood in terms of interchain coherent hopping along b, i.e., 1D-2D crossover around $T_{\max}^b$.

IV. DISCUSSIONS AND CONCLUSION

The small, yet positive MR seen in the resistivity upturn regime in this quasi-1D metal is remarkable. This positive TMR apparently rules out the Kondo scattering as the origin of the low-T upturn in $Ta_{1.2}Os_{0.8}Te_4$. Also, the electron scattering is not strong enough to place this material in the strong localization shrine. In the weak-localization regime, a magnetic field usually gives rise to a negative TMR. However, in their pioneering work, Lee *et al.* proposed that the weakly disordered electron gases may also have positive MR arising from the spin splitting of conduction electron energies in a field and in the high-field regime, this positive MR is supposed to grow as ln$H$ in two dimensions and $\sqrt{H}$ in three dimensions [50,51]. Nevertheless, due to the limit of field strength used in this study, we are unable to test this high-field scaling of MR in $Ta_{1.2}Os_{0.8}Te_4$.

The low-T resistivity upturn as well as the positive TMR may have a common origin with that in disordered quasi-1D $PrBa_2Cu_4O_8$ [45]. In the case of $PrBa_2Cu_4O_8$, the dimensional crossover scenario is regarded as a possible explanation. In this picture, localization appears simultaneously with a dimensional crossover in the electronic ground state when the scattering rate in the chains exceeds the hopping integral between the chains, $\hbar/\tau > 2t_\perp$. The intrachain scattering is so strong that the Bloch wave function cannot propagate between chains, making the electrical transport between chains incoherent; meanwhile, the presence of sufficient amounts of in-chain disorder leads immediately to the localization of in-chain electrons. This leads to the resistivity upturn along *all three* orthogonal directions. In the localized regime of disordered $PrBa_2Cu_4O_8$, a large TMR (orders of magnitude larger than in $Ta_{1.2}Os_{0.8}Te_4$) was observed. This can be understood in terms of "interrupted strand" model [52,53], where the 1D chains are segmented into metallic islands by impurities such that the quasiparticles remain extended over several unit cells and subject to the Lorentz force, inducing the sizable orbital MR [45,54,55]. The same localization physics might also be applicable for $Ta_{1.2}Os_{0.8}Te_4$ here.

In conclusion, we have successfully synthesized the high quality single crystals of a new off-stoichiometric vdW telluride $Ta_{1.2}Os_{0.8}Te_4$. Its 2D atomic layer comprises the alternating arrays of $TaTe_2$ and $OsTe_2$ chains with 20% extra Ta atoms occupying the Os atomic sites. The two interchain resistivities ρ_b and ρ_c show a metal-insulator transition at different temperatures, suggestive of successive crossovers from 3D to 1D with increasing temperature. Multiple physical mechanisms, which possibly give rise to the observed low-T upturn of the resistivity along *all* three crystallographic directions, are discussed. Our results not only suggest that the coupling between chains in $Ta_{1.2}Os_{0.8}Te_4$ forms a 3D FL ground state at low temperatures, consistent with the renormalization group theory, but also provides additional support for the validity of the PF's argument in the dimensional crossover. In the future, it would be intriguing to investigate the physical properties of the stoichiometric vdW telluride $TaOsTe_4$, and explore possible superconductivity, topological physics, or even topological superconductivity therein, given its isostructure to the type-II Weyl semimetal WTe_2 and (Ta, Nb)$IrTe_4$.

ACKNOWLEDGMENTS

The authors would like to thank J. K. Bao for his constructive suggestions on the single-crystal diffraction experiment.

This work was supported by the National Natural Science Foundation of China (Grant No. 11974061) and Zhejiang Provincial Natural Science Foundation of China (Grant No. LY19A040002). S.L.H. would like to acknowledge the financial support from the National Natural Science Foundation of China (Grants No. 11674367, No. 11974364, and No. U2032207). G.-H.C. acknowledges support from the Key R&D Program of Zhejiang Province, China (2021C01002).

[1] D. L. Duong, S. J. Yun, and Y. H. Lee, van der Waals layered materials: Opportunities and challenges, ACS Nano **11**, 11803 (2017).

[2] J. G. Bednorz, and K. A. Müller, Possible high T_c superconductivity in the Ba-La-Cu-O system, Z. Phys. B **64**, 189 (1986).

[3] Y. Kamihara, T. Watanebe, M. Hirano, and H. Hosono, Iron-based layered superconductor La[$O_{1-x}F_x$]FeAs with $T_c = 26$K, J. Am. Chem. Soc. **130**, 3296 (2008).

[4] S. Zhou, L. You, H. L. Zhou, Y. Pu, Z. G. Gui, and J. L. Wang, Van der Waals layered ferroelectric $CuInP_2S_6$: Physical properties and device applications, Front. Phys. **16**, 13301 (2021).

[5] X. F. Qian, J. Liu, L. Fu, and J. Li, Quantum spin Hall effect in two-dimensional transition metal dichalcogenides, Science **346**, 1344 (2014).

[6] F. M. Wang, T. A. Shifa, P. Yu, P. He, Y. Liu, F. Wang, Z. Wang, X. Zhan, X. Lou, F. Xia, and J. He, New frontiers on van der Waals layered metal phosphorous trichalcogenides, Adv. Funct. Mater. **28**, 1802151 (2018).

[7] D. Voiry, R. Fullon, J. Yang, C. Silva, R. Kappera, I. Bozkurt, D. Kaplan, M. J. Lagos, P. E. Batson, G. Gupta, A. D. Mohite, L. Dong, D. Er, V. B. Shenoy, T. Asefa, and M. Chhowalla, The role of electronic coupling between substrate and 2D MoS_2 nanosheets in electrocatalytic production of hydrogen, Nat. Mater. **15**, 1003 (2016).

[8] P. Monceau, Electronic crystals: an experimental overview, Adv. Phys. **61**, 325 (2012).

[9] S. Tomonaga, Remarks on Bloch's method of sound waves applied to many-Fermion problems, Prog. Theor. Phys. **5**, 544 (1950).

[10] J. M. Luttinger, An exactly soluble model of a many-Fermion system, J. Math. Phys. **4**, 1154 (1963).

[11] N. E. Hussey, M. N. McBrien, L. Balicas, J. S. Brooks, S. Horii, and H. Ikuta, Three-Dimensional Fermi-Liquid Ground State in the Quasi-One-Dimensional Cuprate $PrBa_2Cu_4O_8$, Phys. Rev. Lett. **89**, 086601 (2002).

[12] M. N. Mcbrien, N. E. Hussey, P. J. Meeson, S. Horii, and H. Ikuta, Metallic c-axis transport across insulating planes in $PrBa_2Cu_4O_8$, J. Phys. Soc. Jpn. **71**, 701 (2002).

[13] G. Mihály, I. Kézsmárki, F. Zámborszky, and L. Forró, Hall Effect and Conduction Anisotropy in the Organic Conductor $(TMTSF)_2PF_6$, Phys. Rev. Lett. **84**, 2670 (2000).

[14] L. Taillefer, Scattering and pairing in cuprate superconductors, Annu. Rev. Condens. Matter Phys. **1**, 51 (2010).

[15] A. A. Abrikosov and I. A. Ryzhkin, Conductivity of quasi-one-dimensional metal systems, Adv. Phys. **27**, 147 (1978).

[16] C. Castellani, C. Di Castro, and W. Metzner, Instabilities of Anisotropic Interacting Fermi Systems, Phys. Rev. Lett. **69**, 1703 (1992).

[17] V. N. Prigodin and Y. A. Firsov, Pis'ma Zh. Eksp. Teor. Fiz. **38**, 241 (1983) [JETP Lett. **38**, 284 (1983)].

[18] J. W. Su, K. L. Liu, F. K. Wang, B. Jin, Y. B. Guo, G. H. Liu, H. Q. Li, T. and Y. Zhai, Van der Waals 2D transition metal tellurides, Adv. Mater. Interfaces **6**, 1900741 (2009).

[19] W. H. Jiao, Z. T. Tang, Y. L. Sun, Y. Liu, Q. Tao, C. M. Feng, Y. W. Zeng, Z. A. Xu, and G. H. Cao, Superconductivity in a Layered $Ta_4Pd_3Te_{16}$ with $PdTe_2$ Chains, J. Am. Chem. Soc. **136**, 1284 (2014).

[20] W. H. Jiao, L. P. He, Y. Liu, X. F. Xu, Y. K. Li, C. H. Zhang, N. Zhou, Z. A. Xu, S. Y. Li, and G. H. Cao, Superconductivity in $Ta_3Pd_3Te_{14}$ with quasi-one-dimensional $PdTe_2$ chains, Sci. Rep. **6**, 21628 (2016).

[21] W. H. Jiao, X. M. Xie, Y. Liu, X. F. Xu, B. Li, C. Q. Xu, J. Y. Liu, W. Zhou, Y. K. Li, H. Y. Yang, S. Jiang, Y. K. Luo, Z. W. Zhu, and G. H. Cao, Topological Dirac states in a layered telluride $TaPdTe_5$ with quasi-one-dimensional $PdTe_2$ chains, Phys. Rev. B **102**, 075141 (2020).

[22] W. H. Jiao, S. Z. Xiao, B. Li, C. Q. Xu, X. M. Xie, H. Q. Qiu, X. F. Xu, Y. Liu, S. J. Song, W. Zhou, H. F. Zhai, X. Ke, S. L. He, and G. H. Cao, Anisotropic transport and de Haas–van Alphen oscillations in quasi-one-dimensional $TaPtTe_5$, Phys. Rev. B **103**, 125150 (2021).

[23] C. Q. Xu, Y. Liu, P. G. Cai, B. Li, W. H. Jiao, Y. L. Li, J. Y. Zhang, W. Zhou, B. Qian, X. F. Jiang, Z. X. Shi, R. Sankar, J. L. Zhang, F. Yang, Z. W. Zhu, P. Biswas, D. Qian, X. L. Ke, and X. F. Xu, Anisotropic transport and quantum oscillations in the quasi-one-dimensional $TaNiTe_5$: Evidence for the nontrivial band topology, J. Phys. Chem. Lett. **11**, 7782 (2020).

[24] Y. Liu, C. Q. Xu, W. H. Jiao, P. G. Cai, B. Li, W. Zhou, B. Qian, X. F. Jiang, K. R, R. Sankar, X. L. Ke, G. H. Cao, and X. F. Xu, Anisotropic transport in a possible quasi-one-dimensional topological candidate: $TaNi_2Te_3$, Tungsten (2021), doi: 10.1007/s42864-021-00098-2.

[25] K. Koepernik, D. Kasinathan, D. V. Efremov, S. Khim, S. Borisenko, B. Büchner, and J. van den Brink, $TaIrTe_4$: A ternary type-II Weyl semimetal, Phys. Rev. B **93**, 201101(R) (2016).

[26] E. Haubold, K. Koepernik, D. Efremov, S. Khim, A. Fedorov, Y. Kushnirenko, J. van den Brink, S. Wurmehl, B. Büchner, T. K. Kim, M. Hoesch, K. Sumida, K. Taguchi, T. Yoshikawa, A. Kimura, T. Okuda, and S. V. Borisenko, Experimental realization of type-II Weyl state in noncentrosymmetric $TaIrTe_4$, Phys. Rev. B **95**, 241108(R) (2017).

[27] W. Zhou, B. Li, C. Q. Xu, M. R. van Delft, Y. G. Chen, X. C. Fan, B. Qian, N. E. Hussey, and X. F. Xu, Nonsaturating magnetoresistance and nontrivial band topology of type-II Weyl semimetal $NbIrTe_4$, Adv. Electron. Mater. **5**, 1900250 (2019).

[28] Y. Xing, Z. B. Shao, J. Ge, J. H. Wang, Z. W. Zhu, J. Liu, Y. Wang, Z. Y. Zhao, J. Q. Yan, D. Mandrus, B. H. Yan, X. J. Liu, M. H. Pan, and J. Wang, Surface superconductivity in the type-II Weyl semimetal $TaIrTe_4$, Natl. Sci. Rev. **7**, 579 (2020).

[29] Y. L. Li, Z. Ran, C. Z. Huang, G. Y. Wang, P. Y. Shen, H. L. Huang, C. Q. Xu, Y. Liu, W. H. Jiao, W. X. Jiang, J. Y. Hu, G. C. Zhu, C. H. Xu, Q. Lu, G. H. Wang, Q. Jing, S. Y. Wang, Z. W. Shi, J. F. Jia, X. F. Xu, W. T. Zhang, W. D. Luo, and D. Qian, Coexistence of ferroelectric-like polarization and Dirac-like surface state in $TaNiTe_5$, arXiv:2106.09426.

[30] A. A. Soluyanov, D. Gresch, Z. Wang, Q. Wu, M. Troyer, X. Dai, and B. A. Bernevig, Type-II Weyl semimetals, Nature (London) **527**, 495 (2015).

[31] Y. Wu, D. X. Mou, N. H. Jo, K. W. Sun, L. Huang, S. L. Bud'ko, P. C. Canfield, and A. Kaminski, Observation of Fermi arcs in the type-II Weyl semimetal candidate WTe_2, Phys. Rev. B **94**, 121113(R) (2016).

[32] See Supplemental Material at http://link.aps.org/supplemental/10.1103/PhysRevB.105.064201 for details on the determinations of the chemical composition, the independent atomic sites, thermal displacement parameters, and the related bond lengths and bond angles of $Ta_{1.2}Os_{0.8}Te_4$.

[33] G. M. Sheldrick, A short history of SHELX, Acta Crystallogr. A **64**, 112-122 (2008).

[34] A. Mar, S. Jobic, and J. A. Ibers, Metal-metal vs tellurium-tellurium bonding in WTe_2 and its ternary variants $TaIrTe_4$ and $NbIrTe_4$, J. Am. Chem. Soc. **114**, 8963 (1992).

[35] G. Shipunov, B. R. Piening, C. Wuttke, T. A. Romanova, A. V. Sadakov, O. A. Sobolevskiy, E. Yu. Guzovsky, A. S. Usoltsev, V. M. Pudalov, D. Efremov, S. Subakti, D. Wolf, A. Lubk, B. Büchner, and S. Aswartham, Layered van der Waals topological metals of $TaTMTe_4$ (TM = Ir, Rh, Ru) family, J. Phys. Chem. Lett. **12**, 6730 (2021).

[36] A. Narduzzo, A. Enayati-Rad, P. J. Heard, S. L. Kearns, S. Horii, F. F. Balakirev, and N. E. Hussey, Fragile three-dimensionality in the quasi-one-dimensional cuprate $PrBa_2Cu_4O_8$, New J. Phys. **8**, 172 (2006).

[37] Z. Ovadyahu, Y. Gefen, and Y. Imry, Dimensionality crossover induced by a magnetic field in thin metallic films, Phys. Rev. B **32**, 781 (1985).

[38] C. E. Filippini, J. Beille, M. Boujida, J. Marcus, and C. Schlenker, Physica C **162-164**, 427 (1989).

[39] J. Lu, X. Xu, M. Greenblatt, R. Jin, P. Tinnemans, S. Licciardello, M. R. van Delft, J. Buhot, P. Chudzinski, and N. E. Hussey, Emergence of a real-space symmetry axis in the magnetoresistance of the one-dimensional conductor $Li_{0.9}Mo_6O_{17}$, Sci. Adv. **5**, eaar8027 (2019).

[40] A. P. Petrovic, D. Ansermet, D. Chernyshov, M. Hoesch, D. Salloum, P. Gougeon, M. Potel, L. Boeri, and C. Panagopoulos, A disorder-enhanced quasi-one-dimensional superconductor, Nat. Commun. **7**, 12262 (2016).

[41] N. F. Mott and E. A. Davis, *Electronic Processes in Non-Crystalline Materials* (Clarendon Press, Oxford, 1979).

[42] A. Enayati-Rad, A. Narduzzo, F. Rullier-Albenque, S. Horii, and N. E. Hussey, Irradiation-Induced Confinement in a Quasi-One-Dimensional Metal, Phys. Rev. Lett. **99**, 136402 (2007).

[43] I. V. Gornyi, A. D. Mirlin, and D. G. Polyakov, Dephasing and Weak Localization in Disordered Luttinger Liquid, Phys. Rev. Lett. **95**, 046404 (2005).

[44] J. Kondo, Resistance minimum in dilute magnetic alloys, Prog. Theor. Phys. **32**, 37 (1964).

[45] A. Narduzzo, A. Enayati-Rad, S. Horii, and N. E. Hussey, Possible Coexistence of Local Itinerancy and Global Localization in a Quasi-One-Dimensional Conductor, Phys. Rev. Lett. **98**, 146601 (2007).

[46] M. Harris, Y. F. Yan, P. Matl, N. P. Ong, P. W. Anderson, T. Kimura, and K. Kitazawa, Violation of Kohler's Rule in the Normal-State Magnetoresistance of $YBa_2Cu_3O_{7-\delta}$ and $La_2Sr_xCuO_4$, Phys. Rev. Lett. **75**, 1391 (1995).

[47] N. P. Ong, Geometric interpretation of the weak-field Hall conductivity in two-dimensional metals with arbitrary Fermi surface, Phys. Rev. B **43**, 193 (1991).

[48] M. Lee, Y. Suzuki, and T. H. Geballe, Coexistence of metallic and nonmetallic charge transport in $PrBa_2Cu_3O_7$, Phys. Rev. B **51**, 15619 (1995).

[49] I. Terasaki, N. Seiji, S. Adachi, and H. Yamauchi, Low-temperature charge transport in $PrBa_2Cu_4O_8$: Electronic states of the doped Cu-O chain, Phys. Rev. B **54**, 11993 (1996).

[50] P. A. Lee and T. V. Ramakrishnan, Magnetoresistance of weakly disordered electrons, Phys. Rev. B **26**, 4009 (1982).

[51] P. A. Lee and T. V. Ramakrishnan, "Disordered electronic systems," Rev. Mod. Phys. **57**, 287 (1985).

[52] D. Kuse and H. R. Zeller, Evidence for One-Dimensional Metallic Behavior in $K_2Pt(CN)_4Br_{0.3} \cdot (H_2O)_n$, Phys. Rev. Lett. **27**, 1060 (1971).

[53] M. J. Rice and J. Bernasconi, Interrupted strand model for quasi one dimensional metals, J. Phys. F **3**, 55 (1973).

[54] X. F. Xu, A. F. Bangura, J. G. Analytis, J. D. Fletcher, M. M. J. French, N. Shannon, J. He, S. Zhang, D. Mandrus, R. Jin, and N. E. Hussey, Directional Field-Induced Metallization of Quasi-One-Dimensional $Li_{0.9}Mo_6O_{17}$, Phys. Rev. Lett. **102**, 206602 (2009).

[55] N. Dupuis and G. Montambaux, Localization and magnetic field in a quasi-one-dimensional conductor, Phys. Rev. B **46**, 9603 (1992).